Redox-Linked Hydrogen Bond Strength Changes in Cytochrome *a*: Implications for a Cytochrome Oxidase Proton Pump†

Gerald T. Babcock* and Patricia M. Callahan

ABSTRACT: The heme *a* formyl group of cytochrome *a* in cytochrome oxidase appears to be involved in a hydrogen-bond interaction with a proton donor associated with the polypeptide backbone [Callahan, P. M., & Babcock, G. T. (1983) *Biochemistry 22*, 452–461]. Resonance Raman and optical absorption spectroscopies have been applied to the beef heart and *Thermus thermophilus* proteins and to heme *a* and copper porphyrin *a* models in order to assess the spectroscopic manifestations and the energetics of the hydrogen-bond interaction. We find a linear relationship between optical absorption red shift and carbonyl vibrational frequency decrease for a series of hydrogen-bonded model complexes; the magnitude of both changes increases as the hydrogen-bond strength increases. Comparison of the model compound data with analogous data for the proteins indicates that the strength of the formyl hydrogen bond in situ increases by 2–2.5 kcal/mol upon reduction of ferric cytochrome *a*. The selective stabilization of reduced cytochrome *a* by the stronger hydrogen bond is expected to increase the redox potential of this center; the energy made available as the hydrogen bond strengthens during reduction may be used to drive redox-coupled events in the protein. Thus, the linkage between cytochrome *a* redox state and chromophore/protein interaction energy provides a mechanism by which electron-transfer events and protein structure are coupled. Two models, which incorporate this linkage into a redox-driven proton pump centered at cytochrome *a* in cytochrome oxidase, are presented.

To reduce dioxygen efficiently during mitochondrial respiration, cytochrome oxidase uses two copper/heme *a* iron pairs. One pair, cytochrome a_3 and Cu_{a_3}, forms the dioxygen reducing site in the protein. The second pair, cytochrome *a* and Cu_a, is involved in mediating the electron-transfer reaction between cytochrome *c* and the a_3/Cu_{a_3} pair. In addition, Wikström and co-workers and several other research groups have suggested that proton translocation is coupled to the cyt a/Cu_a electron-transfer function and thus that these components form a redox-linked proton pump in the enzyme [see Wikström et al. (1981) for a review].

While the existence of the proton pump appears to be accepted by most researchers in the field [see, however, the recent article by Mitchell & Moyle (1983)], the mechanism by which redox change is coupled to proton translocation remains obscure. Wikström et al. (1981) presented arguments implicating cyt *a* and suggested a reciprocating site model for its involvement. Chan et al. (1979), on the other hand, interpreted the unusual spectroscopic, and hence structural, properties of Cu_a as an indication of unusual function and proposed a fairly detailed model demonstrating the plausibility of a Cu_a-based pump. While Cu_a and cyt *a* appear to be associated with subunits I and II of the oxidase, recent biochemical work has implicated subunit III in proton translocation (Casey et al., 1980). The generality of its role is uncertain, however, owing to the occurrence of a proton pump in the two-subunit oxidase from *Paracoccus denitrificans* (Solioz et al., 1982).

Recently, the unusual spectroscopic properties of cyt *a*, particularly its optical absorption red shift relative to low-spin heme *a* model compounds, have been interpreted in terms of the structure for its heme *a* chromophore shown in Figure 1, where –XH denotes a proton-donating group associated with the polypeptide backbone (Callahan & Babcock, 1983). We report here that the strength of the hydrogen bond between the formyl oxygen and the proton donor depends on the redox state of the cyt *a* iron. This redox-linked shift in hydrogen-bond strength provides a mechanism by which electron-transfer events at the metal can be coupled to protein-based proton translocation; we discuss two different mechanisms for this coupling.

Materials and Methods

Beef heart cytochrome oxidase and heme *a* were isolated from mitochondria as described previously (Babcock & Salmeen, 1979). The reduction of heme *a* model compounds in aprotic solvents was carried out as described by Van Steelandt-Frentrup et al. (1981). The iron atom was removed from the heme *a* moiety and copper inserted to form copper(II) porphyrin *a* by using procedures given by Fuhrop & Smith (1975). Optical (McPherson EU-707D or Cary 17D spectrophotometers) and electron paramagnetic resonance (Bruker 200D EPR spectrometer) spectroscopies were used to assay product formation. Solvents were spectral grade and were dried over molecular sieves prior to use; other reagents were obtained commercially and, when necessary, were further purified by distillation. Resonance Raman spectroscopy was carried out at room temperature on model compounds or at 4 °C on protein samples as described previously (Callahan & Babcock, 1983). Raman peak positions are accurate to ±1.5 cm^{-1}; optical peak positions are accurate to ±0.5 nm.

Results

Figure 2 shows Soret excitation Raman spectra of oxidized and reduced beef heart cytochrome oxidase and of the reduced protein isolated from *Thermus thermophilus* (Fee et al., 1980) in the 1500–1700-cm^{-1} frequency region. Also included in the figure are Raman spectra of ferric and ferrous heme *a*–$(NMeIm)_2$,[1] a cyt *a* model compound (Callahan & Babcock, 1981), in a non-hydrogen-bonding solvent. In the proteins,

† From the Department of Chemistry, Michigan State University, East Lansing, Michigan 48824-1322. *Received February 8, 1983.* This work was supported by National Institutes of Health Grant GM25480.

[1] Abbreviations: EPR, electron paramagnetic resonance; $(NMeIm)_2$, bis(*N*-methylimidazole); cyt, cytochrome; Hepes, 4-(2-hydroxyethyl)-1-piperazineethanesulfonic acid; HiPIP, high-potential iron–sulfur protein.

0006-2960/83/0422-2314$01.50/0

Table I: Spectroscopic Characteristics of Hydrogen-Bonded Heme *a* and Copper(II) Porphyrin *a* Species

no.	species	λ_{max}^{α} [a] (nm)	$\Delta\bar{\nu}_{\alpha}$ [b] (cm^{-1})	$\bar{\nu}_{C=O}$ [c] (cm^{-1})	$\Delta\bar{\nu}_{C=O}$ [d] (cm^{-1})	ΔH_{HB} [e] (kcal/mol)
1	cytochrome a^{3+}	598	284	1650	20	3.0
2	heme a^{3+}-$(NMeIm)_2$ in CH_2Cl_2	588		1670		
3	heme a^{3+}-$(NMeIm)_2$ in CH_2Cl_2 + phenol-d_6	595	200	1652	18	2.7
4	heme a^{3+}-$(NMeIm)_2$ in trichloroethanol	595	200	1654	16	2.4
5	heme a^{3+}-$(NMeIm)_2$ in methanol	589	30	1666	4	0.6
6	cytochrome a^{2+}	604	480	1610	35	5.3
7	heme a^{2+}-$(NMeIm)_2$ in CH_2Cl_2	587		1645		
8	heme a^{2+}-$(NMeIm)_2$ in H_2O	594	201	1633	12	1.8
9	heme a^{2+}-$(NMeIm)_2$ in CH_2Cl_2 + phenol-d_6	598	313	1622	23	3.5
10	Cu^{2+} porphyrin *a* in CH_2Cl_2	596		1666		
11	Cu^{2+} porphyrin *a* in CH_2Cl_2 + trifluoroacetic acid	613	465	1640	26	3.9
12	Cu^{2+} porphyrin *a* in trichloroethanol	606	277	1649	17	2.6
13	Cu^{2+} porphyrin *a* in CH_2Cl_2 + *p*-chlorophenol	607	304	1642	24	3.6
14	Cu^{2+} porphyrin *a* in CH_2Cl_2 + phenol-d_6	606	277	1642	24	3.6

[a] α-Band optical absorption maximum. [b] Frequency difference in α-band optical absorption maxima for the indicated compound and the corresponding non-hydrogen-bonded species. [c] Formyl carbonyl stretching frequency. [d] Frequency difference in carbonyl stretching frequencies for the indicated compound and the corresponding non-hydrogen-bonded species. [e] Hydrogen bond strength as calculated from eq 1.

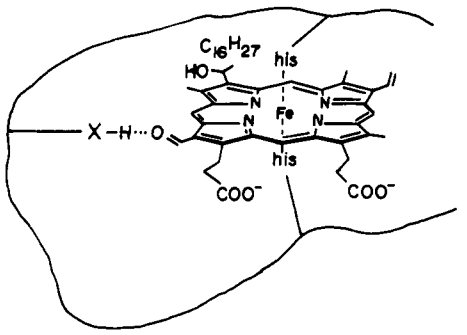

FIGURE 1: Postulated active-site structure for cytochrome *a* in cytochrome oxidase. The heme *a* iron is six-coordinate with histidines occupying the two axial ligation sites. The peripheral formyl group is involved in a hydrogen bond with a proton donor designated as X–H, which is associated with the polypeptide backbone.

the formyl vibration occurs at 1676 cm^{-1} for cyt a_3^{3+} and decreases to 1665 cm^{-1} for cyt a_3^{2+}. This behavior is typical of high-spin heme *a* model compounds in aprotic solvents and indicates that the carbonyl group of cyt a_3 is isolated in a hydrophobic environment in both of its valence states (Van Steelandt-Frentrup et al., 1981; Babcock et al., 1981). The formyl vibrational frequencies for cyt *a* (Callahan & Babcock, 1983) and its model compounds are indicated by vertical lines in the figure. For both valence states, the in situ carbonyl shows a significant frequency decrease compared to its corresponding model compound. This decrease amounts to 20 cm^{-1} for oxidized cyt *a* and to 35 cm^{-1} for the reduced center. The *Thermus* protein shows an analogous decrease which, along with similar data for rat liver cytochrome oxidase (Babcock et al., 1981), indicates that the lower in situ frequency is not a peculiarity of the beef enzyme.

Shifts in carbonyl vibrational frequencies of this magnitude are commonly observed upon hydrogen-bond formation (Murthy & Rao, 1968). Moreover, because the visible and Soret optical absorption bands of heme *a* are π–π^* transitions that involve the formyl as part of the π system, an absorption red shift should accompany hydrogen-bond formation. Both the magnitude of the formyl vibrational frequency decrease and of the absorption red shift should increase as the strength of the hydrogen bond increases (Pimentel & McClellan, 1960). The proportionality between carbonyl frequency decrease and absorption red shift appears to hold for cyt *a* in its two valence states. For the ferric form, the α-band absorption maximum is shifted by 10 nm (284 cm^{-1}) to 598 nm relative to its non-hydrogen-bonded model, and the carbonyl frequency decrease is 20 cm^{-1} (Table I). For the ferrous form, the absorption red shift relative to the non-hydrogen-bonded model is greater, 17 nm (480 cm^{-1}), and likewise the vibrational

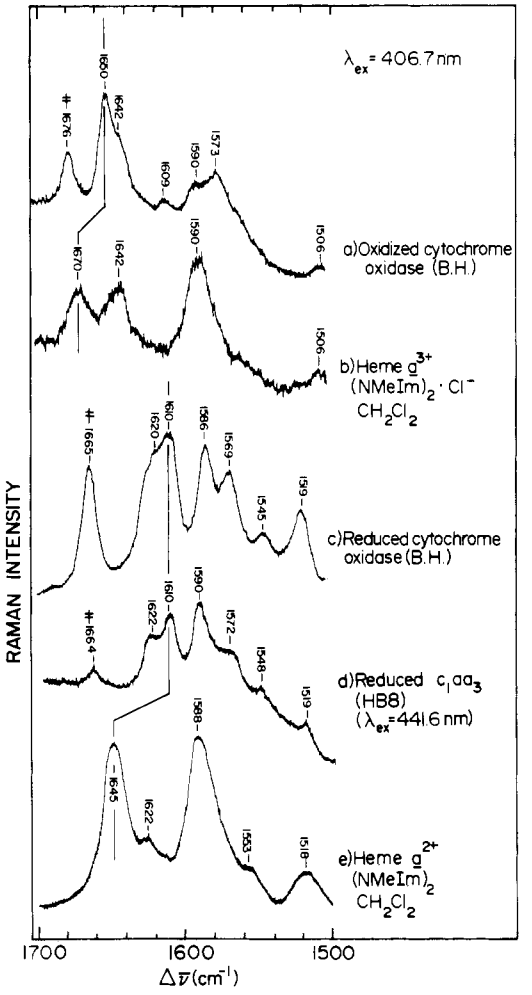

FIGURE 2: High-frequency Soret excitation Raman spectra of cytochrome oxidase and low-spin heme *a* model compounds. In (a) and (c), the beef heart enzyme, dissolved in 0.05 M Hepes/0.5% lauryl maltoside, pH 7.4, was used. In (d) cytochrome oxidase (c_1aa_3) from *T. thermophilus* in the Hepes/maltoside buffer was used. In (b) and (e) the bis(*N*-methylimidazole)–heme *a* complex was dissolved in methylene chloride. The carbonyl stretching frequency for cytochrome a_3 is indicated by a ‡ in (a), (c), and (d).

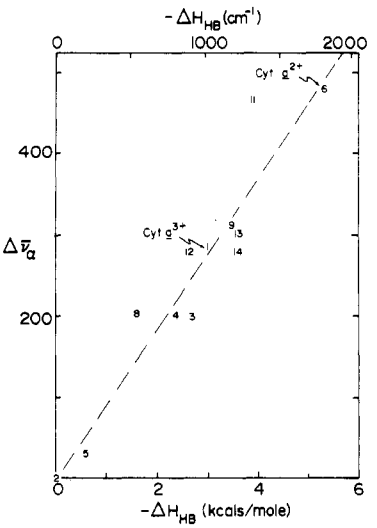

FIGURE 3: Absorption red shift for cytochrome *a*, heme *a*, or copper porphyrin *a* species as a function of hydrogen-bond enthalpy as calculated from eq 1. The points are numbered according to the compounds listed in Table I.

frequency is decreased by 35 cm^{-1}.

To explore the coupling between the carbonyl vibrational frequency, the optical absorption red shift, and the hydrogen-bond strength in cyt *a* in more detail, we recorded optical and Raman spectra for several low-spin heme *a* and copper porphyrin *a* model compounds in different solvents and in the presence of various hydrogen donors. We used copper porphyrin *a* to obtain spectroscopic parameters for the chromophore in the presence of more acidic donors. These cannot be used with heme *a*–$(NMeIm)_2$ because they protonate N_ϵ of the iron ligand, which results in the formation of the high-spin heme *a* complex. We also used deuterated rather than protonated phenol as a donor in order to avoid overlap of its vibrations with those of the porphyrin macrocycle in the high-frequency region. Table I summarizes the results in terms of α-band maximum, carbonyl frequency, and hydrogen-bond strength (see below) for the models and for cyt *a*. In Figure 3, the absorption red shift is plotted as a function of both the carbonyl frequency decrease and the calculated hydrogen-bond strength. The approximately linear relationship apparent in the figure is typically what one observes in correlating hydrogen-bonding phenomena in a series of loosely related compounds (Arnett et al., 1974).

Discussion

From the formyl frequency shift observed upon hydrogen-bond formation, an estimate of the strength of the hydrogen bond for the heme *a* species under consideration can be made. This relies upon a variation of the Badger–Bauer rule, which has been widely applied to vibrational data obtained for the hydrogen donor involved in the bond [e.g., Pimentel & McCellan (1960)]. The corresponding relationship for the acceptor is (Zadorozhnyi & Ishchenko, 1965)

$$\Delta\bar{\nu}_{C=O}/\bar{\nu}_{C=O} = -K_{C=O}\Delta H_{HB} \qquad (1)$$

where ΔH_{HB} is the hydrogen-bond enthalpy, $K_{C=O}$ is a proportionality constant, $\bar{\nu}_{C=O}$ is the vibrational frequency of the free (non-hydrogen-bonded) carbonyl, and $\Delta\bar{\nu}_{C=O}$ is the difference in vibrational frequency between the free and the hydrogen-bonded acceptor. By use of a series of aldehydes, ketones, and carboxylic acids as acceptors and phenols or alcohols as donors, a value of $K_{C=O} = 4 \times 10^{-3}$ mol/kcal has been estimated (Zadorozhnyi & Ishchenko, 1965). Realizing that this value is likely to hold only roughly for heme *a* species, particularly for the diverse class of donors in Table I (Arnett et al., 1974), we have used it to estimate ΔH_{HB} for the various complexes. These are given in the table and are used in Figure 3 to obtain the correlation between hydrogen-bond strength and absorption red shift. When the hydrogen-bond enthalpy is expressed in wavenumbers, the slope of the least-squares line drawn in the figure is 0.28. This value is within the range one expects for the proportionality between hydrogen-bond strength and the π–π^* transition red shift which results (Pimentel & McClellan, 1960).

From the data in Table I and Figure 3, it is apparent that both ferric and ferrous cyt *a* have optical, vibrational, and hydrogen-bond enthalpy characteristics which are consistent with the model compounds. An important conclusion follows from this observation because it indicates that the major protein-induced modification of the chromophore occurs by hydrogen bonding to the formyl group.[2] Moreover, the hydrogen-bonding effects are more pronounced for cyt a^{2+} than for cyt a^{3+}. Because the hydrogen bond strengthens upon reduction, the redox potential of cyt *a* is more positive than it would be in the absence of such an interaction. Modulation of the hydrogen-bond strength in situ for either oxidized or reduced cyt *a* may provide an explanation for the unusual redox properties of the heme *a* components of cytochrome oxidase [e.g., Babcock et al. (1978)].

The chemical basis for the difference in hydrogen-bond enthalpy for the two cyt *a* valence states is straightforward. Sheridan, Allen, and their co-workers have investigated redox dependencies in hydrogen-bond strength for both heme and FeS proteins (Valentine et al., 1979; Sheridan et al., 1981). In heme proteins, where they explored the iron ligand histidine as a proton donor, the ferric state is stabilized by hydrogen-bond formation. In FeS proteins, where the metal ligand is a hydrogen acceptor, they noted stronger hydrogen bonds for the reduced cluster. The porphyrin *a* ligand to iron in cyt *a* resembles the FeS protein case in that it is a proton acceptor, and we expect stronger hydrogen bonding in the ferrous state; i.e., upon reduction of the iron the electron density on the carbonyl oxygen increases, and it becomes a better proton acceptor. Cyt *a* behaves this way in situ, and it is also observed when heme *a* model compounds are considered. For example, the hydrogen bond formed between phenol and low-spin heme *a* is stronger by ~0.8 kcal/mol when the iron is in the ferrous, as opposed to the ferric, valence state (Table I). The increased negative charge at the carbonyl oxygen in ferrous heme *a* is also apparent in that a 25-cm^{-1} decrease in carbonyl stretching frequency, presumably due to population of the π^* antibonding orbital, is observed for ferrous heme *a* models compared to ferric heme *a* in the absence of hydrogen-bonding effects (Figure 2).

Given the approximate nature of eq 1, we calculate that the hydrogen bond strength change which occurs on redox cycling of cyt *a* is in the neighborhood of 2–2.5 kcal/mol (90–110 mV). This energy is comparable to the electrochemical proton gradient against which protons are translocated in mitochondria [estimated to lie between 160 and 230 mV with a best value of around 200 mV (Wikström et al., 1981)], particularly if the hydrogen bond strength change is augmented by other redox-linked processes, e.g., a shift in electrostatic potential at the heme (Warshel & Weiss, 1981) or additional

[2] Other perturbations, for example, shifts in the electrostatic potential at the heme (Warshel & Weiss, 1981) or point charge effects (Honig et al., 1979), may influence the optical spectrum as well, but these effects appear to be small compared to the hydrogen-bonding interaction.

hydrogen-bond contributions from the cyt *a* axial histidines (Valentine et al., 1979; Babcock et al., 1979). Alternatively, one could envision a situation in which both cyt *a*, as discussed below, and Cu_a, as suggested by Chan et al. (1979), operate as proton pumps in which the duty cycle for each would be one-half. Before discussing possible pump models for cyt *a*, however, it is necessary to consider the relationship between the hydrogen-bond enthalpy changes we have observed and the free energy actually made available for proton translocation. In the early literature on hydrogen-bond formation, increases in hydrogen-bond strength (decreases in $\Delta H°_f$) for a series of hydrogen-bonded structures appeared to be accompanied by decreases in $\Delta S°_f$ so that the free energy change remained somewhat constant (Pimentel & McClellan, 1960). More recently, and arguing from a much larger data set, Arnett and co-workers (Arnett et al., 1974) concluded that such a generalization is not justified in that a hydrogen-bond reaction series may be essentially isoentropic yet show large changes in $\Delta H°_f$. In these cases, the change in $\Delta H°_f$ will be reflected in a change in $\Delta G°_f$. Such a situation is likely to occur in cyt *a* owing to the fact that the major contribution to the decrease in $\Delta S°_f$ for a reaction series where it is observed is usually attributed to loss of translational entropy upon complexation. Because the proton donor to the cyt *a* formyl is most likely immobilized by its polypeptide environment, the translational entropy will be small regardless of the hydrogen-bond strength. Thus we expect that changes in cyt *a* hydrogen-bond enthalpy will be accompanied by a free energy change of a comparable magnitude and that this will be available for proton pumping.

From a variety of models in which the redox-driven change in cyt *a* hydrogen-bond strength could be used to translocate protons, we will consider two. In the first, the free energy change at the formyl serves as a switch that produces a conformational change in a different region of the protein that allows proton conduction. In the second, the proton hydrogen-bonded to the carbonyl is an integral component of a proton wire and is actually pumped during the redox cycle. Relevant to both of these models is the relationship between hydrogen-bond strength and hydrogen-bond geometry discussed by Valentine et al. (1979). The geometry is determined by two factors: the distance, *r*, between the heavy atoms involved in the hydrogen bond and the angular deviation of the bond, α, from linearity. With these definitions, the hydrogen-bond strength is proportional to $\cos \alpha / r$.

In the first model, the reduction of cyt *a* leads to a decrease in either *r* or α (or both). The change in local structure about the heme *a* chromophore is transmitted to the proton-translocating section of the protein where a conformational change resulting in proton translocation occurs. Supporting this model is the observation that the major conformation change, which occurs upon reduction of cytochrome oxidase, is controlled by the redox state of cyt *a* (Cabral & Love, 1972). A second piece of potentially supporting evidence comes from the observation that dissociation of cytochrome oxidase subunit III abolishes the pH dependence in the midpoint potential of cyt *a* in the cyanide-inhibited enzyme (Artzatbanov et al., 1978; Penttilä & Wikström, 1981). The possible mechanics of proton conduction as related to a conformation change have been considered in detail by Nagle & Morowitz (1978). The mechanism by which the hydrogen bond geometry change at the heme *a* site is transmitted through the protein to the pumping section may bear some resemblance to that proposed by Perutz & Brunori (1982) for the control of the Root effect in fish hemoglobins.

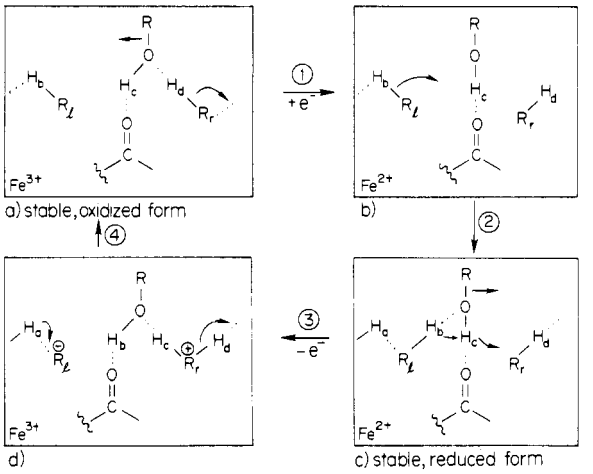

FIGURE 4: A possible mechanism for the redox-driven proton pump in cytochrome oxidase. The cytochome *a*–heme *a* moiety is indicated by Fe >C=O; the iron valence is indicated. In (a), the stable oxidized form of the cyt *a* site is indicated. A hydrogen-bonded chain in its higher energy configuration occurs to the right of the formyl group and is designated as H_d–R_r···; a hydrogen-bonded chain in its lower energy configuration occurs to the left of the formyl group and is designated as ···H_b–R_l. Reduction is shown as a two-step process that results in (c), the stable reduced form of the site. The arrows in (a) and (b) indicate the changes in structure that occur during steps 1 and 2, respectively. Reoxidation occurs by a two-step process, with (d) as an intermediate, to regenerate the stable, oxidized cyt *a* configuration. The hydrogens involved in the pumping action are subscripted with letters a–d to identify their motions during the various steps.

The second model represents a direct mechanism for proton translocation in that the formyl hydrogen-bonded proton is pumped during the redox cycle. This kind of mechanism requires that covalent bonds involving hydrogen and the polypeptide heavy atom in the formyl hydrogen bond are made and broken during proton translocation. Because resonance Raman can provide vibrational information on only the chromophore moiety of a protein, we have no direct insight as to the identity of the proton donor to the cyt *a* carbonyl. However, we suspect that it is an –OH group from either an alcohol or a carboxylic acid side chain. An $-NH_2$ group is much less likely owing to the facility with which amines form Schiff base linkages with heme *a* (Ward et al., 1983), and –SH groups can be eliminated owing to the extremely weak hydrogen bonds they form (Perutz & Brunori, 1982).

With these considerations, the mechanism in Figure 4, which is similar in certain aspects to the switch model for bacteriorhodopsin proposed by Nagle & Mille (1981), can be postulated. In Figure 4a, the stable form of ferric cyt *a* is shown, where a fairly weak (3 kcal/mol) hydrogen bond exists between the peripheral C=O and the –OH donor. As indicated in the figure, the weak hydrogen bond assumes a nonlinear geometry ($\alpha \neq 0°$). Two proton-donating groups, R_r–H_d and R_l–H_b, are located in the immediate vicinity of the cyt *a* carbonyl. R_r–H_d is connected to the right-hand side of the membrane by an asymmetric hydrogen-bonded chain, and R_l–H_b is similarly connected to the left side of the membrane (Nagle & Morowitz, 1978; Nagle & Mille, 1981). On the right-hand side R_r–H_d is shown in the oxidized, resting form of the enzyme (Figure 4a) with H_d hydrogen bonded to the oxygen of the donor group to cytochrome *a*. This interaction determines the configurational energy of the hydrogen-bond chains, and in Figure 4a, the interaction R–O···H_d–R_r holds the right-hand side proton chain in its high-energy conformation. The left-hand side proton chain is in its low-energy form.[3]

Proton pumping proceeds from left to right. Reduction of the iron results in a two-step change in the hydrogen-bond geometry and produces the stable reduced form of cyt *a* shown in Figure 4c. In the first step, process 1, reduction of the iron leads to greater electron density at the carbonyl oxygen. As a result, the C=O···H_c—O hydrogen bond strengthens as it shifts to a more linear configuration. The O···H_d–R_r hydrogen bond breaks, and the right side of the chain relaxes to its lower energy configuration. Proton release on the right side may occur at this step, but it is not necessary. In the second step, the –OH_c oxygen, which has become a stronger proton acceptor as a result of the strengthening of the OH_c···O=C hydrogen bond (Huyskens, 1977), stabilizes the higher energy configuration in the left side chain as the R_l–H_b···O hydrogen bond forms. Situations similar to this, i.e., ones in which an amino acid side chain acts as both a hydrogen donor and a hydrogen acceptor, do not appear to be unusual. Serine in fish hemoglobins (Perutz & Brunori, 1982) and tyrosine in HiPIP (Sheridan et al., 1981) provide two examples. Moreover, the two processes are correlated in that as the donor hydrogen bond strengthens, the acceptor hydrogen bond will also strengthen (Huyskens, 1977). The result of reduction, then, produces the configuration shown in Figure 4c. Upon oxidation of cyt *a*, the two-step process shown in steps 3 and 4 returns the site to its resting oxidized conformation. In step 3, the OH_c···O=C hydrogen bond weakens as the ROH_c group shifts right to its relaxed configuration. As this occurs, the H_c···R_r bond forms and strengthens. The H_b···O hydrogen bond continues to strengthen as a result of this process and becomes covalent. The result is the state shown in Figure 4d. Although localized positive and negative charges are shown on R_r and R_l, respectively, they need not occur if the covalent bond-breaking/bond-making processes are closely coupled. In the final step in the process, step 4, the R_l^- group picks up a proton from the left (H_a) to become neutral and returns to the resting low-energy conformation. On the right, the $R_r{}^+H_2$ loses a proton to the right and is stabilized in the higher energy conformation by the O···H–R_r hydrogen bond.

The essential feature of the model of Figure 4 is the redox-linked switch from high-energy configuration of the asymmetric hydrogen-bonded chain on the right and low-energy configuration on the left to the opposite conformation, i.e., low energy on the right and high energy on the left. Relaxation of this state as oxidation occurs resets the system for a second cycle of proton translocation. One further point should be emphasized for this model. The 2–2.5 kcal/mol associated with cytochrome *a* hydrogen bond strength changes is not enough energy to make the proton pump significantly irreversible under steady-state conditions in mitochondria. For this to occur, other redox-coupled events (e.g., those suggested above) must also contribute to the overall free energy required to make the pump thermodynamically feasible. The situation thus becomes analogous to the Warshel & Weiss (1981) view of hemoglobin, where both chemical bond strength change (i.e., "strain") and electrostatic processes were proposed to contribute to the free energy difference between the R state and the T state. Within this context, the model of Figure 4 postulates the switching element and a source for part of the energy required to drive a proton pump in cytochrome oxidase.

[3] The concept of hydrogen-bonded chains has been developed by Nagle and co-workers (Nagle & Morowitz, 1978; Nagle & Mille, 1981). Such a chain could conceivably span protein subunits so the involvement of subunit III in cytochrome oxidase proton translocation may be accommodated by this model as well.

Acknowledgments

We thank Profs. J. A. Fee for providing samples of the *T. thermophilus* protein and M. Wikström and S. I. Chan for several helpful discussions.

Registry No. Cytochrome *a*, 9035-34-1; cytochrome oxidase, 9001-16-5; hydrogen ion, 12408-02-5; ferric heme *a*–$(NMeIm)_2$, 85236-37-9; ferrous heme *a*–$(NMeIm)_2$, 85236-38-0; Cu^{2+} porphyrin *a*, 85236-39-1.

References

Arnett, E. M., Mitchell, E. J., & Murty, T. S. S. R. (1974) *J. Am. Chem. Soc. 96*, 3875–3891.

Artzatbanov, V. Yu., Konstantinov, A. A., & Skulachev, V. P. (1978) *FEBS Lett. 87*, 180–185.

Babcock, G. T., & Salmeen, I. (1979) *Biochemistry 18*, 2493–2498.

Babcock, G. T., Vickery, L. E., & Palmer, G. (1978) *J. Biol. Chem. 253*, 2400–2411.

Babcock, G. T., Van Steelandt, J., Palmer, G., Vickery, L. E., & Salmeen, I. (1979) *Dev. Biochem. 5*, 105–115.

Babcock, G. T., Callahan, P. M., Ondrias, M. R., & Salmeen, I. (1981) *Biochemistry 20*, 959–966.

Cabral, F., & Love, B. (1972) *Biochim. Biophys. Acta 283*, 181–184.

Callahan, P. M., & Babcock, G. T. (1981) *Biochemistry 20*, 952–958.

Callahan, P. M., & Babcock, G. T. (1983) *Biochemistry 22*, 452–461.

Casey, R. P., Thelen, M., & Azzi, A. (1980) *J. Biol. Chem. 255*, 3994–4000.

Chan, S. I., Bocian, D. F., Brudvig, G. W., Morse, R. H., & Stevens, T. H. (1979) *Dev. Biochem. 5*, 177–188.

Fee, J. A., Choc, M. G., Findling, K.-L., Lorence, R., & Yoshida, T. (1980) *Proc. Natl. Acad. Sci. U.S.A. 77*, 147–151.

Fuhrop, J. H., & Smith, K. M., Eds. (1975) *Laboratory Methods in Porphyrin and Metalloporphyrin Research*, p 42, Elsevier/North-Holland, Amsterdam.

Honig, B., Dinur, U., Nakanishi, K., Balogh-Nair, V., Gawinowicz, M. A., Arnaboldi, M., & Motto, M. G. (1979) *J. Am. Chem. Soc. 101*, 7084–7086.

Huyskens, P. L. (1977) *J. Am. Chem. Soc. 99*, 2578–2582.

Mitchell, P., & Moyle, J. (1983) *FEBS Lett. 151*, 167–178.

Murthy, A. S. N., & Rao, C. N. R. (1968) *Appl. Spectrosc. Rev. 2*, 69–191.

Nagle, J. F., & Morowitz, H. J. (1978) *Proc. Natl. Acad. Sci. U.S.A. 75*, 298–302.

Nagle, J. F., & Mille, M. (1981) *J. Chem. Phys. 74*, 1367–1372.

Penttilä, T., & Wikström, M. (1981) in *Vectorial Reactions in Electron and Ion Transport in Mitochondria and Bacteria* (Palmieri, F., et al., Eds.) pp 71–80, Elsevier/North-Holland, Amsterdam.

Perutz, M. F., & Brunori, M. (1982) *Nature (London) 299*, 421–426.

Pimentel, G. C., & McClellan, A. L. (1960) *The Hydrogen Bond*, W. H. Freeman, San Francisco.

Sheridan, R. P., Allen, L. C., & Carter, C. W., Jr. (1981) *J. Biol. Chem. 256*, 5052–5057.

Solioz, M., Carafoli, E., & Ludwig, B. (1982) *J. Biol. Chem. 257*, 1579–1582.

Valentine, J. S., Sheridan, R. P., Allen, L. C., & Kahn, P. C. (1979) *Proc. Natl. Acad. Sci. U.S.A. 76*, 1009–1013.

Van Steelandt-Frentrup, J., Salmeen, I., & Babcock, G. T. (1981) *J. Am. Chem. Soc. 103*, 5981–5982.

Ward, B., Callahan, P. M., Young, R., Babcock, G. T., & Chang, C. K. (1983) *J. Am. Chem. Soc. 105*, 634–636.
Warshel, A., & Weiss, R. M. (1981) *J. Am. Chem. Soc. 103*, 446–451.
Wikström, M., Krab, K., & Saraste, M. (1981) *Annu. Rev. Biochem. 50*, 623–655.
Zadorozhnyi, B. A., & Ishchenko, I. K. (1965) *Opt. Spectrosc. (Engl. Transl.) 19*, 306–308.

Single-Channel Recordings from Purified Acetylcholine Receptors Reconstituted in Bilayers Formed at the Tip of Patch Pipets†

Benjamin A. Suarez-Isla,‡ Kee Wan, Jon Lindstrom, and Mauricio Montal*

ABSTRACT: The channel of the purified acetylcholine receptor from *Torpedo californica* electric organ reconstituted in lipid vesicles was assayed by direct electrical recording using patch-clamp pipets. High-resistance seals were obtained by gentle suction of vesicles into the pipet or after the formation of lipid bilayers from monolayers at the tip of the pipet. Single-channel currents were activated by three cholinergic ligands: acetylcholine, carbamylcholine, and suberyldicholine. The single-channel conductance, γ, was 40 ± 5 pS in 0.5 M NaCl, irrespective of the agonist used. The distributions of channel open times were fitted by a sum of two exponentials. The lifetimes of the two exponential components were a factor of 2 longer for suberyldicholine than for acetylcholine or carbamylcholine. At desensitizing concentrations of agonists the single events appeared in paroxysms of channel activity followed by quiescent periods. These results suggest that the full cycle of solubilization, purification, and reconstitution of this membrane receptor can be achieved without impairment of channel function.

Understanding the mechanism of action of channel proteins depends on the convergence of knowledge about the structure of the protein with the detailed characterization of its function at the molecular level. The nicotinic acetylcholine receptor of postsynaptic membranes provides an opportunity to pursue this goal.

Acetylcholine receptor from the electroplax of the ray *Torpedo californica* has been purified and extensively characterized. It is a pentamer of approximate molecular weight 270 000 with a subunit composition of $\alpha_2\beta\gamma\delta$ [reviewed in Anholt et al. (1983), Karlin (1980), Changeux (1981), and Raftery et al. (1980)]. Recently, the amino acid sequences of all four subunits have been elucidated (Noda et al., 1982, 1983; Claudio et al., 1983). The purified receptor has been reconstituted in lipid vesicles [Huganir et al., 1979; Changeux et al., 1979; Lindstrom et al., 1980; Anholt et al., 1980, 1981, 1982; cf. Anholt et al. (1983)] and in planar lipid bilayers (Nelson et al., 1980; Boheim et al., 1981; Labarca et al., 1982, 1983; P. Labarca, J. Lindstrom, and M. Montal, unpublished results). These studies demonstrated that the $\alpha_2\beta\gamma\delta$ subunit structure of the receptor contains both the agonist binding sites and the cation channel that they regulate [cf. Anholt et al. (1983)].

Purified receptors in reconstituted vesicles exhibit two salient features of the postsynaptic membrane, namely, activation and desensitization induced by cholinergic agonists [cf. Anholt et al. (1983)]. These activities are assayed by measuring the translocation of radioactive cations in response to the addition of cholinergic agonists. Although such measurements are convenient and simple, they lack the sensitivity and time resolution needed to study the opening and closing of individual receptor channels. Therefore, it would be of significant interest to study the current fluctuations produced by activation of receptor channels in the same reconstituted vesicles that are used in biochemical assays.

Three recent technical advances allowed us to record the activity of the receptor channel electrophysiologically in reconstituted vesicles: (a) the transfer of *purified* AChR from reconstituted vesicles into monolayers at the air–water interface was demonstrated (Labarca et al., unpublished results); (b) lipid bilayers have been formed from monolayers at the air–water interface in the tip of patch pipets by the successive removal of the pipet from the water and reimmersion through the interface (Wilmsen et al., 1982; Hanke et al., 1983; Coronado & Latorre, 1983); (c) the patch-clamp recording technique (Neher & Sakmann, 1976; Hamill et al., 1981; Horn & Patlak, 1980) has been adapted to record Cl^- channels from crude extracts of *Torpedo* electroplax incorporated into large liposomes (Tank et al., 1982).

Here, we present preliminary results demonstrating the use of patch pipets to obtain single-channel recordings from *purified* receptor reconstituted in vesicles after formation of high-resistance seals (gigaohm range) by gentle suction of the vesicles into the pipet and by the formation of a reconstituted bilayer from monolayers at the tip of the pipet.

Experimental Procedures

Receptor Preparation and Solutions. Receptor from the electric organ of *T. californica* (Pacific Biomarine, Venice,

† From the Departments of Biology and Physics (B.A.S.-L. and M.M.), University of California, San Diego, La Jolla, California 92093, and The Receptor Biology Laboratory (K.W. and J.L.), The Salk Institute for Biological Studies, San Diego, California 92138. *Received February 14, 1983.* This investigation was supported by research grants from the National Institutes of Health (EY-02084 to M.M. and NS 11323 to J.L.), the Office of Naval Research (N00014-79-C-0798 to M.M. and J.L.), the Department of the Army Medical Research (17-82-C221 to M.M.), the Muscular Dystrophy Association of America (to J.L.), and the McKnight Foundation (to J.L.). During the course of this study M.M. was a John Simon Guggenheim Foundation Fellow.

‡ Permanent address: Laboratory of Neurosciences, National Institutes of Health, National Institute on Aging, Baltimore City Hospitals, Baltimore, MD 21224.

0006-2960/83/0422-2319$01.50/0